Deterministic emitter-cavity coupling using a single-site controlled quantum dot

Dan Dalacu,* Khaled Mnaymneh, Vera Sazonova, Philip J. Poole, Geof C. Aers, Jean Lapointe, Ross Cheriton, Anthony J. SpringThorpe, and Robin Williams

Institute for Microstructural Sciences, National Research Council, Ottawa, Canada K1A 0R6

(Received 4 May 2010; revised manuscript received 27 May 2010; published 12 July 2010)

Site-selective epitaxy is used to deterministically control the nucleation site of a single quantum dot. A photonic crystal cavity is fabricated at the dot site for a true single quantum dot-cavity system which, by design, contains no background emitters. Cavity tuning at fixed temperature is used to measure the dot-cavity coupling over a large (>15 meV) detuning range using nonresonant excitation. The low-excitation spectra are modeled using a master equation model based on incoherent excitation. We find that pure phonon dephasing alone does not account for the observed nonresonant cavity emission and an additional cavity feeding mechanism, consistent with phonon-assisted dot-cavity coupling, must be included to reproduce the experimental spectra.

DOI: 10.1103/PhysRevB.82.033301 PACS number(s): 73.21.La, 78.67.Hc

Efficient sources of single photons and entangled photon pairs are required for applications in quantum information processing and quantum key distribution as well as for fundamental experiments that test the foundations of quantum mechanics.[1–3] Quantum dots, coupled to semiconductor microcavities, are viewed as a promising solid-state implementation of a nonclassical light source. A decade after the first realization of a coupled single dot-cavity system,[4,5] fabrication of devices is becoming increasingly routine[6–12] and additional experiments consistently point to differences between quantum dots and their atomic counterpart, in particular, the role of the environment in the solid state.

In the atomic case, emission is mainly peaked at the emitter energy regardless of detuning and there is no cavity mode emission when there is negligible overlap between the dot and cavity linewidths. In the solid state, one observes nonresonant emitter-cavity coupling[6,7] even for significant detunings.[8,9] Nonresonant cavity emission is predicted from fast dephasing processes,[13–15] multiexciton transitions,[9] and exciton-phonon coupling[16] and is expected to be dependent on excitation type and rate, electron-phonon interactions, charge fluctuations, etc. Nonresonant coupling has major implications for quantum information processing[10,15] and one needs to understand the physics responsible for the optical response of these solid-state emitter-cavity systems. For experiments targeted at coupling single quantum dots to localized cavity modes, complications arise due to the statistical nature of the quantum dot self-assembly process; it is simply difficult to control where individual quantum dots are located. Cavity feeding from background emitters[7] masks the very processes that one would like to investigate.

In this Brief Report, we study dot-cavity coupling using devices based on site-controlled quantum dots.[17] Direct control of the nucleation site of the dot provides systematic spatial matching for true scalability, in contrast to deterministic approaches[18–20] based on registration of randomly nucleated dots. The devices studied here are single-dot devices by design and one can unambiguously rule out the presence of background emitters. Using photonic crystal cavities, we study the dot-cavity coupling for detunings up to 15 meV. Spectral matching is achieved without adjusting the sample temperature,[21,22] thereby eliminating the tuning dependence of electron-acoustic phonon interactions.[7,10,11] The measured spectra are analyzed using a master equation theory relevant for incoherent excitation.[23] We find that pure dephasing alone does not account for the observed nonresonant cavity emission near resonance, and an additional cavity feeding mechanism, consistent with phonon-assisted coupling, is required to reproduce the measured spectra. In contrast to previous results[8,9] no cavity emission is observed at low-excitation powers for detunings >5 meV, suggesting that cavity feeding from multiexciton transitions does not play a role in these experiments. We also explicitly show the influence of phonon interactions on the nonresonant dot-cavity coupling using temperature-dependent measurements at constant detuning.

A schematic of the device is shown in Fig. 1(a). Quantum dot site control is achieved through selective-area epitaxy[24] which is used to direct the self-assembly process in the InAs/InP quantum dot material system. The fabrication process

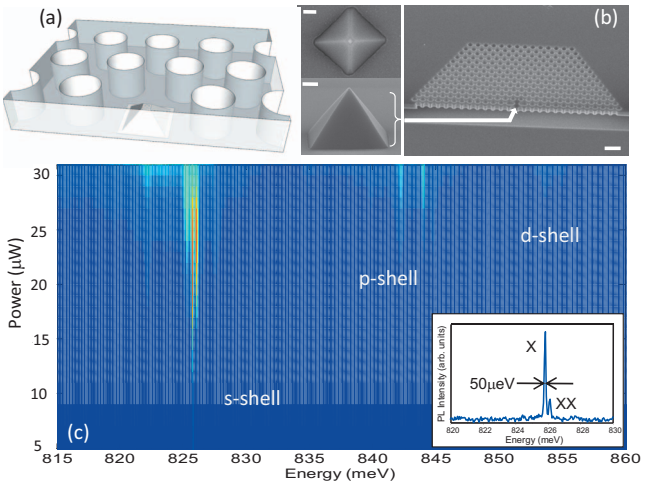

FIG. 1. (Color) (a) Schematic of the site-controlled single dot-cavity device. (b) SEM images of device at different stages of fabrication. Top left: plan view of an uncapped InP pyramid showing the InAs quantum dot on the (001) top facet. Bottom left: oblique view of a capped InP pyramid. Right: cross-section of the photonic crystal cavity. Scale bars for left (right) images are 100 nm (1 μm). (c) Excitation spectra of a site-controlled quantum dot showing bound *s*, *p*, and *d* orbitals. The inset shows a representative low excitation spectrum.

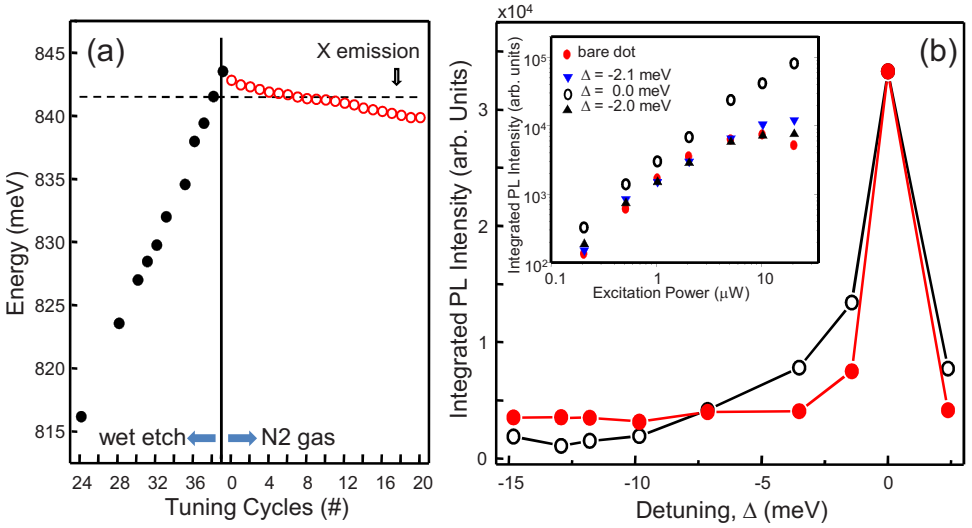

FIG. 2. (Color online) (a) Cavity mode energy during tuning. (b) Integrated PL intensity of the cavity (open black circles) and dot (filled red circles) versus detuning. Inset shows the power-dependent integrated PL intensity of the dot prior to cavity fabrication (bare dot) and for the dot-cavity system near and at resonance.

involves nucleation of a single InAs quantum dot at the apex of an InP pyramid as shown in the scanning electron microscopy (SEM) image in Fig. 1(b). The pyramid is grown on a SiO_2 patterned InP wafer with a thin InP buffer layer over a 1 μm thick lattice matched InAlAs sacrificial layer. The pyramid is in registry with alignment marks etched into the substrate, allowing fabrication of a two-dimensional (2D) photonic crystal membrane nanocavity with an optical defect precisely positioned at the quantum dot. An alignment precision of better than 50 nm is determined from SEM images on test structures. Individual dots are characterized prior to cavity fabrication, allowing for the cavity design to be tailored to each dot. Figure 1(c) shows typical power-dependent spectra from a site-selected quantum dot. We note the absence of background emitters: the spacing of pyramids is arbitrary and, for the samples studied here, is set to 200 μm. A low pump power emission spectrum using above band-gap excitation shows only a single peak over the entire spectral range available to our spectrometer/detector setup, $\lambda = 1.1-1.7$ μm.

Cavity fabrication involves planarization of the InP pyramid, dry etching of the holes and wet etching of the InAlAs sacrificial layer to release the resulting membrane. The cavity design is based on a modified single missing hole defect[25] that is robust against process- and tuning-induced variations of the cavity geometry, with Q-values of 10 000–15 000.[26] Optical measurements are done at 4.2 and 40 K in a continuous flow helium cryostat using nonresonant, above band-gap excitation through a 50X microscope objective (N.A. =0.42). The photoluminescence (PL) is collected by the same objective, dispersed using a single grating spectrometer and detected using a liquid nitrogen cooled InGaAs array.

For spectral matching of the dot and cavity, a two-step process is used: (i) coarse cavity tuning to high energy followed by (ii) fine tuning to low energy. The as-fabricated cavity is designed with the mode on the low energy side of the dot emission. The cavity is tuned through resonance in 1.7 meV steps using a digital wet etching technique which involves sequential cycles of InP native oxide growth and subsequent removal.[21] The cavity is then tuned back through resonance in arbitrarily fine steps using inert gas condensation.[22] Figure 2(a) shows the tuning process for a dot emitting at 842 meV. The as-fabricated cavity mode energy was well below 800 meV. Pumping at saturation, $P = P_{sat}$, it takes 24 wet etch cycles for the cavity mode to appear at 816 meV and a total of 39 cycles to take the cavity one cycle past the dot emission. From higher energy the cavity is tuned back though the dot by condensing N_2 gas on the surface of the crystal with the size of the tuning steps dictated by the volume of gas condensed per cycle. For the case shown in Fig. 2(a), the cavity was tuned back to 840 meV in 100 μeV steps.

The integrated PL intensity of the dot and cavity emission for different wet etch cycle number, plotted as a function of dot-cavity detuning, is shown in Fig. 2(b) for excitation at saturation, $P = P_{sat}$. The dot emission remains approximately constant for large detunings, the intensity dictated by vertical background radiation leakage into modes above the light line.[27] At zero detuning, dot-cavity coupling is evident from the enhanced dot emission. A second signature of coupling is the modification of the saturation behavior of the dot near resonance shown in the inset of Fig. 2(b). Already at detunings of ± 2 meV, the onset of saturation of the exciton transition has started to shift to higher excitation powers from a cavity-mediated reduction in lifetime[28] while at zero detuning there is no sign of saturation for the largest excitation powers used. The significant cavity mode emission observed for detunings up to $\Delta = 10$ meV is not associated with the ground state emission, but rather with cavity feeding from multiexciton complexes[29] (biexciton and transitions associated with population of the p shell) and concomitant emission lines which appear around the ground state at high excitation rates, see Fig. 1(c).

PL spectra as a function of N_2 tuning are shown as a contour plot in Fig. 3(a) for a dot emitting at 830 meV. In this case, the excitation power is well below saturation, P

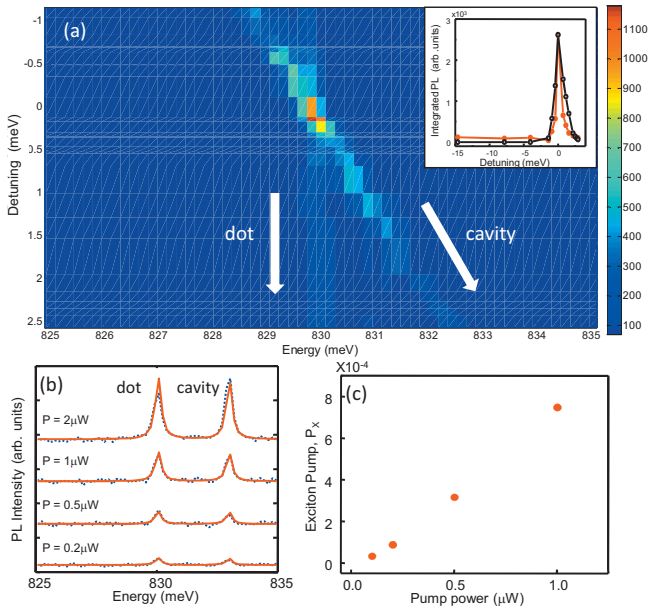

FIG. 3. (Color) (a) Low pump power PL spectra tuned using N_2. Inset shows the integrated intensity of the cavity (open black circles) and dot (filled red circles) over the entire detuning range. (b) Measured (dotted blue curves) and fit (red curves) excitation-dependent emission spectra for $\Delta=3$ meV. (c) Incoherent pump rate dependence on experimental power extracted from (b).

$=0.02P_{sat}$, to avoid cavity feeding from higher level excitations, and no cavity emission is observed for detunings greater than 5 meV (see inset) as one would expect if there are no extraneous pumping mechanisms. To model the spectra we have used the master equation formalism of Yao *et al.*[23] (see also Laussy *et al.*[30]) which describes the emission from a coupled dot-cavity system under incoherent excitation. The total spectrum is divided into emission via radiation modes above the light line, S_r, and emission from the leaky cavity, S_c:

$$S_c(\omega)=\frac{\Gamma_c}{\pi}Re\left[\frac{i\langle\hat{a}^\dagger\hat{a}\rangle D(\omega)}{C(\omega)D(\omega)-g^2}+\frac{ig\langle\hat{a}^\dagger\hat{\sigma}^-\rangle}{C(\omega)D(\omega)-g^2}\right] \quad (1)$$

$$S_r(\omega)=\frac{\Gamma_x}{\pi}Re\left[\frac{i\langle\hat{a}^\dagger\hat{a}\rangle C(\omega)}{C(\omega)D(\omega)-g^2}+\frac{ig\langle\hat{\sigma}^+\hat{a}\rangle}{C(\omega)D(\omega)-g^2}\right], \quad (2)$$

where $C(\omega)=\omega-\omega_c+\frac{i}{2}\Gamma_c$ and $D(\omega)=\omega-\omega_x+\frac{i}{2}(2P_x+\Gamma_x+\Gamma_x')$. ω_c and ω_x are the cavity and dot resonance frequencies, respectively, Γ_c is the decay rate of the cavity, Γ_x and Γ_x' are the exciton radiative decay and pure dephasing rates, respectively, and g is the dot-cavity coupling rate. $\hat{a}$ represents the cavity mode operator and $\hat{\sigma}^{+/-}$ are the Pauli operators of the exciton. The steady-state solutions for the exciton population, $\langle\hat{\sigma}^+\hat{\sigma}^-\rangle$, the cavity photon population, $\langle\hat{a}^\dagger\hat{a}\rangle$, and the cross-term, $\langle\hat{a}^\dagger\hat{\sigma}^-\rangle$, are given by:

$$\langle\hat{a}^\dagger\hat{a}\rangle=\frac{g^2\Gamma(P_x+P_c)+P_c(2P_x+\Gamma_x)\left[\frac{\Gamma^2}{4}+\Delta^2\right]}{g^2\Gamma(2P_x+\Gamma_x+\Gamma_c)+\Gamma_c(2P_x+\Gamma_x)\left[\frac{\Gamma^2}{4}+\Delta^2\right]} \quad (3)$$

$$\langle\hat{a}^\dagger\hat{\sigma}^-\rangle=\frac{-ig\left(\langle\hat{a}^\dagger\hat{a}\rangle-\frac{P_x}{2P_x+\Gamma_x}\right)\left[i\Delta+\frac{\Gamma}{2}\right]}{\frac{\Gamma^2}{4}+\Delta^2+\frac{g^2\Gamma}{2P_x+\Gamma_x}} \quad (4)$$

$$\langle\hat{\sigma}^+\hat{\sigma}^-\rangle=\frac{P_x+ig(\langle\hat{a}^\dagger\hat{\sigma}^-\rangle-\langle\hat{a}\hat{\sigma}^+\rangle)}{\Gamma_x+2P_x}, \quad (5)$$

where $\Gamma=2P_x+\Gamma_x+\Gamma_x'+\Gamma_c$. P_x and P_c are the incoherent exciton and cavity pump rates, respectively, and $\Delta=\omega_c-\omega_x$. The total emission spectrum is given by the sum

$$S_{tot}(r,\omega)=F_r(r)S_r(\omega)+F_c(r)S_c(\omega), \quad (6)$$

where F_r and F_c are geometric factors determined by the collection optics for the emission into radiation and cavity modes, respectively.

We first estimate the ratio F_r/F_c by fitting spectra pumped at different excitation powers when the dot-cavity system is significantly detuned ($\Delta=3$ meV). We note that the measured cavity and dot linewidths are instrument-limited at 250 μeV. We do not use the resolution-limited linewidths, but rather, use the measured linewidths of test structures measured on higher resolution spectrometers, and include the

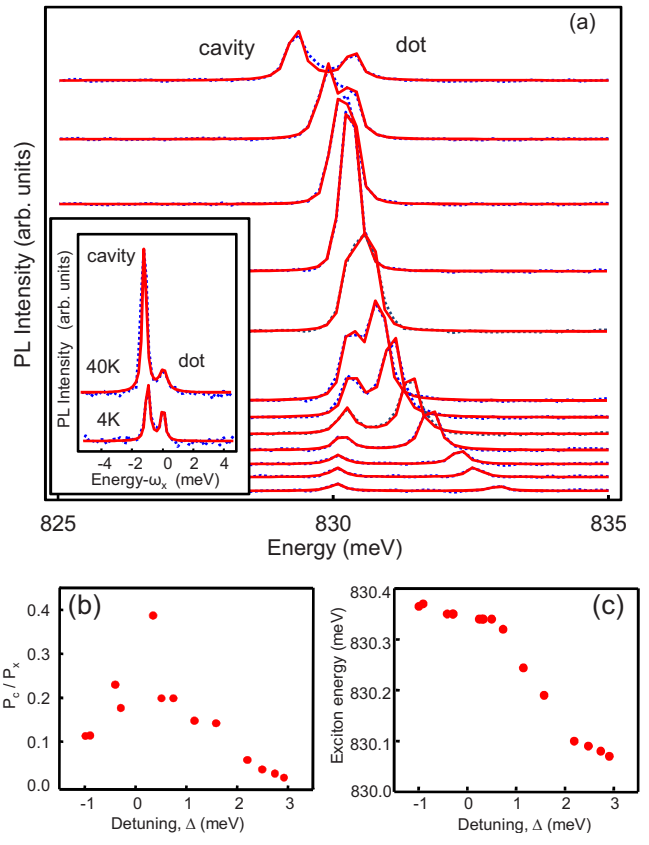

FIG. 4. (Color online) Fits (red curves) of Eq. 7 applied to low pump spectra (dotted blue curves) for detunings available to N_2 condensation. Inset shows spectra for $\Delta=1$ meV at 4 K (40 K) and model fits using $\Gamma_x'=50$ μeV ($\Gamma_x'=575$ μeV). (b) Incoherent cavity pump rates, P_c/P_x, extracted from (a). (c) Detuning-dependent shift of the exciton transition energy.

resolution limit in the model. Γ_c is set to 100 μeV which is a conservative estimate based on test structures fabricated using dot ensembles.[26] Γ_x' is set to 50 μeV, which is the typical measured linewidth of the site-controlled InAs/InP dots [see inset, Fig. 1(c)]. We note that the measurements can be done at 30 K, where the dot-linewidth increases to 250 μeV and is no longer resolution-limited, and our findings are the same. We also note that these parameters put the system into the strong coupling regime, however we do not expect to spectrally resolve the anticrossing given the dot-cavity coupling rate, g (see below).

Γ_x is set to 2 μeV from lifetime measurements on site-controlled InAs/InP dots ($\tau \sim 1$ ns) and only g, P_x, and the ratio F_r/F_c are varied. There is no need to include a cavity pump contribution for this large detuning to reproduce the experimental spectra; the non-resonant cavity emission is fully described by a dephasing rate of $\Gamma_x'=50$ μeV. The excellent fit to the data is shown in Fig. 3(b) from which a value of $F_r/F_c=1/10$ is obtained. This procedure also allows us to calibrate the experimental excitation rate in terms of P_x [Fig. 3(c)] used in all subsequent fits.

To fit the spectra for different detunings, Δ is first determined for each spectrum, then only g and P_c are varied globally (they are applied to all tuning spectra simultaneously). This approach gives excellent agreement only if it is applied separately for large and small detunings. A global fit of P_c overestimates the cavity emission for $\Delta \gtrsim 2$ meV while setting P_c to 0 underestimates the cavity emission for $\Delta \lesssim 2$ meV. As mentioned above, at large detunings P_c is necessarily small. For $\Delta \lesssim 2$ meV, however, the spectra are reproduced by the model only by including a cavity pump contribution of P_c/P_x of ~ 0.4. In order to fit the entire tuning range P_c is set as a detuning-dependent parameter and only g is varied globally. The resulting fits are shown in Fig. 4(a) from which $g=130$ μeV, indicating good spatial matching and is typical of the half dozen dot-cavity samples measured. The extracted P_c values as a function of detuning are plotted in Fig. 4(b). Note that P_c is fit only for detunings for which the emission doublet is resolved, $|\Delta| > 300$ μeV [outside the shaded region in Fig. 4(b)] to avoid correlations between fit parameters. This near-resonance cavity pump term represents a cavity feeding mechanism that is in addition to that expected from a pure dephasing.[10,11] The spectral range over which this dot-cavity coupling is important is consistent with cavity feeding based on phonon-assisted transitions from the exciton to the cavity.[16]

Using the ability to tune independently of temperature, measurements were made of the same dot-cavity sample at 40 K and a detuning $\Delta=1$ meV. The 4 and 40 K spectra are shown in the inset of Fig. 4(a). The increase in cavity emission at the elevated temperature provides proof of the role of phonon-mediated cavity feeding, both pure dephasing[10,11] and exciton-phonon coupling[16] on the nonresonant dot-cavity coupling. The enhanced cavity emission is consistent with the predictions of Eq. (6) and the 40 K spectrum is reproduced with no fitting parameters, the dephasing rate is simply increased to $\Gamma_x'=575$ μeV, in direct correspondence with the experimental linewidth.

As a final remark, we note the detuning-dependent shift of the exciton transition energy observed in Fig. 4(a). This is not reproduced by Eqs. (1) and (2) but has been added as part of the fit of the detuning. The origin of this shift, which amounts to ~ 300 μeV at resonance [Fig. 4(c)] is unclear, but maybe related to cavity-exciton attraction described in Ref. 31.

In conclusion, we have studied the dot-cavity coupling using a site-controlled single quantum dot coupled to a photonic crystal microcavity. We show that the non-resonant cavity emission cannot be described by pure dephasing only, but requires an additional feeding mechanism consistent with a phonon-mediated process that relies on a combined effect of exciton-cavity and exciton-phonon couplings.

This work was partially supported by the Natural Science and Engineering Research Council and Quantumworks.

*dan.dalacu@nrc-cnrc.gc.ca

[1] E. Knill *et al.*, Nature (London) **409**, 46 (2001).
[2] A. Beveratos *et al.*, Phys. Rev. Lett. **89**, 187901 (2002).
[3] P. Hawrylak and M. Korkusiński, Nonlinear Opt. **29**, 329 (2002).
[4] P. Michler *et al.*, Science **290**, 2282 (2000).
[5] C. Santori *et al.*, Nature (London) **419**, 594 (2002).
[6] K. Hennessy *et al.*, Nature (London) **445**, 896 (2007).
[7] D. Press *et al.*, Phys. Rev. Lett. **98**, 117402 (2007).
[8] M. Kaniber *et al.*, Phys. Rev. B **77**, 161303(R) (2008).
[9] M. Winger *et al.*, Phys. Rev. Lett. **103**, 207403 (2009).
[10] S. Ates *et al.*, Nat. Photonics **3**, 724 (2009).
[11] J. Suffczyński *et al.*, Phys. Rev. Lett. **103**, 027401 (2009).
[12] A. Laucht *et al.*, Phys. Rev. Lett. **103**, 087405 (2009).
[13] A. Naesby *et al.*, Phys. Rev. A **78**, 045802 (2008).
[14] M. Yamaguchi *et al.*, Opt. Express **16**, 18067 (2008).
[15] A. Auffèves *et al.*, Phys. Rev. A **79**, 053838 (2009).
[16] U. Hohenester, Phys. Rev. B **81**, 155303 (2010).
[17] D. Chithrani *et al.*, Appl. Phys. Lett. **84**, 978 (2004).
[18] A. Badolato *et al.*, Science **308**, 1158 (2005).
[19] K. H. Lee *et al.*, Appl. Phys. Lett. **88**, 193106 (2006).
[20] A. Dousse *et al.*, Phys. Rev. Lett. **101**, 267404 (2008).
[21] D. Dalacu *et al.*, Appl. Phys. Lett. **87**, 151107 (2005).
[22] S. Mosor *et al.*, Appl. Phys. Lett. **87**, 141105 (2005).
[23] P. Yao *et al.*, Phys. Rev. B **81**, 033309 (2010).
[24] D. Dalacu *et al.*, Laser Photonics Rev. **4**, 283 (2010).
[25] O. J. Painter *et al.*, J. Lightwave Technol. **17**, 2082 (1999).
[26] J. Devenson *et al.*, Appl. Phys. Lett. **89**, 191115 (2006).
[27] S. Hughes and P. Yao, Opt. Exp. **17**, 3322 (2009).
[28] E. M. Purcell, Phys. Rev. **69**, 37 (1946).
[29] M. Korkusinski *et al.*, M. Zielinski, and P. Hawrylak, J. Appl. Phys. **105**, 122406 (2009).
[30] F. P. Laussy *et al.*, Phys. Rev. Lett. **101**, 083601 (2008); Phys. Rev. B **79**, 235325 (2009); E. del Valle *et al.*, *ibid.* **79**, 235326 (2009).
[31] T. Tawara *et al.*, Opt. Express **18**, 2719 (2010).